Stretching, alignment, and shear in slowly varying velocity fields

G. Haller[1] and R. Iacono[2]
[1]*Department of Mechanical Engineering, MIT, Cambridge, Massachusetts 02139, USA*
[2]*ENEA, C.R. Casaccia, Rome, Italy*
(Received 15 April 2003; published 18 November 2003)

We derive criteria that locate intense material stretching and shear in two-dimensional flows with slow time dependence. Our derivation makes use of the near integrability of the equation of variations along trajectories of the slowly varying flow. The criteria yield two diagnostic scalar fields for use in real-time Lagrangian predictions in geophysical flows.

DOI: 10.1103/PhysRevE.68.056304 PACS number(s): 47.52.+j, 47.17.+e

I. INTRODUCTION

In this paper, we derive Lagrangian criteria for regions of material stretching and shear in slowly varying two-dimensional velocity data. Because of their fast convergence, these criteria will be useful in short-term Lagrangian prediction schemes, such as the scheme of Lekien *et al.* [1] for passive pollution control near the surface of Monterey Bay.

A number of studies have addressed the stability of individual fluid trajectories in frames comoving with particles [2–14]. While most studies assume slow variation for the velocity gradient along fluid trajectories, these moving gradients may vary fast even in steady flows. This paper derives Lagrangian stability criteria that are exact for steady flows, regardless of how fast the velocity gradient changes along trajectories. We then apply the same stability criteria to velocity fields that vary slowly in time, expecting that the additional slow variation of velocity gradients due to unsteadiness is negligible, at least over short and intermediate time scales.

We first derive exact criteria for stretching and alignment of material elements in steady flows. Specifically, using Lagrangian velocities and their normal vectors as a basis along trajectories, we solve the equation of variations along a fluid trajectory in the steady limit. The solution leads to a simple stability criterion that identifies repelling, attracting, and neutral trajectories. A side result is an exact formula for the asymptotic alignment direction of material elements at an arbitrary point of the flow. The stability criterion and the alignment formula yield two scalar fields, λ and μ, that highlight stretching, compression, and shear regions in the Lagrangian sense.

As a second step, we extend the results to weakly unsteady velocity fields. In the language of nonlinear dynamics, λ and μ then reveal stable and unstable manifolds, as well as generalized KAM-type regions in two-dimensional slowly varying velocity data. We test our arguments on a two-dimensional barotropic turbulence simulation, finding that λ and μ converge faster than the finite-time Lyapunov exponent distribution, a frequently used Lagrangian stability indicator. Lyapunov exponents highlight both repelling material lines (stable manifolds) and shear lines while missing attracting material lines (unstable manifolds). By contrast, the λ field highlights both stable and unstable manifolds in a single numerical run, distinguishing these manifolds from lines of high shear. As a complementary tool, the μ field locates Lagrangian structures of high shear (such as rings and jets), while it ignores stable and unstable manifolds.

II. THE EQUATION OF VARIATIONS

Consider the two-dimensional velocity field $\mathbf{v}(\mathbf{x},t)=[u(\mathbf{x},t),v(\mathbf{x},t)]^T$, with the associated equation for particle motions,

$$\dot{\mathbf{x}}=\mathbf{v}(\mathbf{x},t), \quad \mathbf{x}\in\mathbb{R}^2. \tag{1}$$

Solutions of this equation are the fluid trajectories $\mathbf{x}(t,\mathbf{x}_0)$ with initial positions $\mathbf{x}(t_0,\mathbf{x}_0)=\mathbf{x}_0$. Small perturbations $\boldsymbol{\xi}=\mathbf{x}_0'-\mathbf{x}_0$ of the initial condition of $\mathbf{x}(t,\mathbf{x}_0)$ satisfy the equation of variations,

$$\dot{\boldsymbol{\xi}}=\nabla\mathbf{v}(\mathbf{x}(t,\mathbf{x}_0),t)\boldsymbol{\xi}. \tag{2}$$

As is well known in the classical theory of ODEs (see, e.g., Hale [15]), a solution of Eq. (2) in the case of *steady* velocity fields is given by

$$\boldsymbol{\xi}(t)=\mathbf{v}(\mathbf{x}(t,\mathbf{x}_0)), \tag{3}$$

as one verifies by direct substitution. While $\mathbf{v}(\mathbf{x}(t,\mathbf{x}_0),t)$ is not a solution to Eq. (2) for unsteady flows, it is still close to a solution for finite times if $\mathbf{v}(\mathbf{x},t)$ varies slowly in time. It is this finite-time closeness that we exploit in our analysis below.

III. PASSAGE TO A MOVING FRAME

Motivated by the solution (3), we introduce a coordinate system whose axes are unit vectors parallel to $\mathbf{v}(\mathbf{x}(t,\mathbf{x}_0))$ and $\mathbf{v}^\perp(\mathbf{x}(t,\mathbf{x}_0))$, a vector orthogonal to $\mathbf{v}(\mathbf{x}(t,\mathbf{x}_0))$. More specifically, we define the vector $\mathbf{v}^\perp$ and the transformation matrix $\mathbf{T}$ as

$$\mathbf{v}^\perp=\begin{pmatrix}-v\\ u\end{pmatrix}, \quad \mathbf{T}(\mathbf{x},t)=\frac{1}{|\mathbf{v}|}[\mathbf{v}(\mathbf{x},t)\mathbf{v}^\perp(\mathbf{x},t)],$$

then fix an initial condition $\mathbf{x}_0$, an initial time t_0, and change coordinates along the trajectory $\mathbf{x}(t,\mathbf{x}_0)$ by letting

$$\boldsymbol{\xi}=\mathbf{T}(\mathbf{x}(t,\mathbf{x}_0),t)\boldsymbol{\eta}.$$

Applying this change of variables to Eq. (2) leads to the transformed equation of variations

$$\dot{\boldsymbol{\eta}}=[\mathbf{A}(t)+b(t)\mathbf{B}]\,\boldsymbol{\eta}, \tag{4}$$

where

$$\mathbf{A}(t)=\begin{pmatrix} S_{\parallel}(t) & a(t) \\ 0 & -S_{\parallel}(t)+\delta(t) \end{pmatrix}, \qquad \mathbf{B}=\begin{pmatrix} 0 & 1 \\ -1 & 0 \end{pmatrix},$$

$$a(t)=\left.\frac{\mathbf{v}\cdot([\boldsymbol{\nabla}\mathbf{v}]\mathbf{v}^{\perp}-[\boldsymbol{\nabla}\mathbf{v}^{\perp}]\mathbf{v})}{|\mathbf{v}|^2}\right|_{\mathbf{x}=\mathbf{x}(t,\mathbf{x}_0)},$$

$$b(t)=\left.\frac{\mathbf{v}^{\perp}\cdot\mathbf{v}_t}{|\mathbf{v}|^2}\right|_{\mathbf{x}=\mathbf{x}(t,\mathbf{x}_0)},$$

$$S_{\parallel}=\left.\frac{(\mathbf{v},\mathbf{S}\mathbf{v})}{|\mathbf{v}|^2}\right|_{\mathbf{x}=\mathbf{x}(t,\mathbf{x}_0)}, \qquad \delta(t)=\boldsymbol{\nabla}\cdot\mathbf{v}|_{\mathbf{x}=\mathbf{x}(t,\mathbf{x}_0)}, \tag{5}$$

with $\mathbf{S}=\frac{1}{2}(\boldsymbol{\nabla}\mathbf{v}+\boldsymbol{\nabla}\mathbf{v}^T)$ denoting the rate-of-strain tensor. Note that $S_{\parallel}$ is the parallel strain rate along the trajectory and $\delta(t)$ is the divergence of the velocity field along the trajectory. The quantity $S_{\parallel}$ has also been used in earlier work to describe growth of disturbances to barotropic steady flows [16].

IV. THE STEADY LIMIT

For slowly varying velocity fields, $(\mathbf{v}^{\perp}\cdot\mathbf{v}_t)/|\mathbf{v}|^2$ is small, and hence Eq. (4) is a small perturbation of its steady limit,

$$\dot{\boldsymbol{\eta}}=\mathbf{A}(t)\,\boldsymbol{\eta}. \tag{6}$$

Equation (4) is also a small perturbation of Eq. (6) if the velocity field is close to the product of a purely time-dependent scalar field and a steady vector field. Below we examine the steady limit (6) more closely.

A. Solutions and invariant manifolds

Direct integration of Eq. (6) gives the solution $\boldsymbol{\eta}(t)=\boldsymbol{\Psi}(t,t_0)\,\boldsymbol{\eta}_0$ with the fundamental solution matrix

$$\boldsymbol{\Psi}(t,t_0)=\begin{pmatrix} \exp\left[\int_{t_0}^{t}S_{\parallel}(\tau)d\tau\right] & \int_{t_0}^{t}\exp\left[\int_{s}^{t}S_{\parallel}(\tau)d\tau\right]\exp\left\{\int_{t_0}^{s}[-S_{\parallel}(\tau)+\delta(\tau)]d\tau\right\}a(s)ds \\ 0 & \exp\left\{\int_{t_0}^{t}[-S_{\parallel}(\tau)+\delta(\tau)]d\tau\right\} \end{pmatrix}. \tag{7}$$

Note that the $\{\eta_2=0\}$ subspace is invariant under the map $\boldsymbol{\Psi}(t,t_0)$, showing that vectors initially tangent to the trajectory $\mathbf{x}(t,\mathbf{x}_0)$ are advected into tangent vectors by the linearized flow. The stability type of the $\{\eta_2=0\}$ subspace is determined by the growth of the η_2 component of vectors initially parallel to the η_2 axis. Specifically, with the notation

$$\lambda(t,t_0)=\int_{t_0}^{t}[-S_{\parallel}(\tau)+\delta(\tau)]\;d\tau$$

$$=\int_{t_0}^{t}\left.\frac{u_x v^2-(u_y+v_x)uv+v_y u^2}{u^2+v^2}\right|_{\mathbf{x}=\mathbf{x}(s,\mathbf{x}_0)}ds, \tag{8}$$

we obtain that

$$\begin{aligned} &\lambda(t,t_0)<0\Rightarrow\{\eta_2=0\}\ \text{ attracts over }\ [t_0,t],\\ &\lambda(t,t_0)>0\Rightarrow\{\eta_2=0\}\ \text{ repels over }\ [t_0,t],\\ &\lambda(t,t_0)=0\Rightarrow\{\eta_2=0\}\ \text{ neutral over }\ [t_0,t], \end{aligned} \tag{9}$$

a general criterion for the stability of a trajectory over the time interval $[t_0,t]$.

The quantity $\lambda(t,t_0)/(t-t_0)$ can be thought of as a finite-Lyapunov exponent computed in the direction orthogonal to the Lagrangian velocity of the trajectory. The exponent $\lambda(t,t_0)$ can also be viewed as a finite-time version of the mixing efficiency proposed by Ottino [17], when the efficiency is evaluated along the unit vector $\mathbf{v}^{\perp}/|\mathbf{v}|$.

B. Hyperbolicity and material alignment

If $\lambda(t,t_0)>0$ holds, then the $\{\eta_2=0\}$ subspace is repelling. At the same time, there is contraction within that subspace, as long as the flow is only moderately compressible, i.e., $\delta(t)<S_{\parallel}(t)$. These two effects imply hyperbolic (saddle-type) behavior for the underlying trajectory $\mathbf{x}(t,\mathbf{x}_0)$ over the time interval $[t_0,t]$. A similar conclusion holds for $\lambda(t,t_0)<0$.

In the $\lambda(t,t_0)>0$ case of hyperbolicity, the zero solution of the linear equation (6) admits a time-dependent unstable manifold W^u. This unstable manifold contains special solutions that converge to the origin as $t\to-\infty$. The manifold W^u is a two-dimensional set in the $(\boldsymbol{\eta},t)$ space-time, with its $t=$const slice $W^u(t)$ forming a line through the origin (see Fig. 1).

The significance of W^u is that all solutions of Eq. (6) outside the $\{\eta_2=0\}$ subspace converge to $W^u(t)$ as $t\to\infty$. As a consequence, typical small perturbations to the initial condition $\mathbf{x}_0$ align asymptotically with $W^u(t)$. Equivalently,

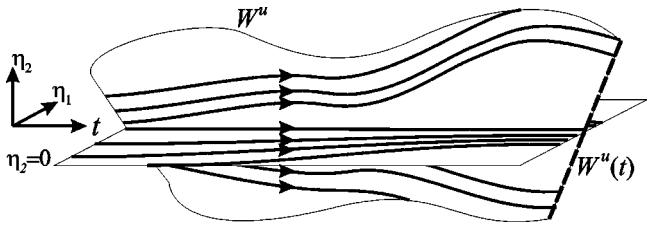

FIG. 1. The unstable manifold W^u in the (η_1,η_2,t) coordinates, and its $t=$const slice $W^u(t)$.

all small material elements placed transversely to $\mathbf{x}(t,\mathbf{x}_0)$ align with $W^u(t)$ as $t\to\infty$.

To find $W^u(t)$ for any t, consider a vector

$$\boldsymbol{\eta}^t=\begin{pmatrix}\eta_1^t\\ \eta_2^t\end{pmatrix}\in W^u(t).$$

By the definition of W^u, all current positions $\boldsymbol{\eta}^t$ in $W^u(t)$ decay to the origin of Eq. (6) in backward time, thus we have

$$\lim_{T\to-\infty}\boldsymbol{\Psi}(T,t)\,\boldsymbol{\eta}^t=\mathbf{0}.$$

Using Eq. (7), we rewrite this last limit as

$$\lim_{T\to-\infty}\left(\eta_1^t\exp\left[\int_t^T S_\parallel(\tau)d\tau\right]+\eta_2^t\int_t^T\exp\left[\int_s^T S_\parallel(\tau)d\tau\right]\right.$$
$$\left.\times\exp\left\{\int_t^s[\delta(\tau)-S_\parallel(\tau)]\;d\tau\right\}a(s)ds\right)=0, \qquad (10)$$

or equivalently,

$$\frac{\eta_1^t}{\eta_2^t}=\lim_{T\to-\infty}\int_T^t\exp\left\{\int_s^t[2S_\parallel(\tau)-\delta(\tau)]d\tau\right\}a(s)ds.$$

Therefore, the angle $\phi(\mathbf{x},t)$ between the velocity $\mathbf{v}(\mathbf{x},t)$ and the instantaneous unstable subspace $W^u(t)$ obeys the formula

$$\cot\phi(\mathbf{x},t)=\lim_{T\to-\infty}\int_T^t\exp\left\{\int_s^t[2S_\parallel(\tau)-\delta(\tau)]\;d\tau\right\}a(s)ds, \qquad (11)$$

where the integrands are to be evaluated along a fluid trajectory that is at the point $\mathbf{x}$ at time t.

The angle $\phi(\mathbf{x},t)$ maintains its meaning for $\lambda(t,t_0)<0$. In that case, the unstable manifold W^u coincides with the $\{\eta_2=0\}$ subspace, and hence $|\cot\phi(\mathbf{x},t)|\to\infty$ as $t\to\infty$. We also recall that the gradients of any tracer field $c(\mathbf{x},t)$ advected by the velocity field align asymptotically with the direction orthogonal to $W^u(t)$. Therefore, the angle $\psi(\mathbf{x},t)$ between the tracer gradient and the velocity field $\mathbf{v}(\mathbf{x},t)$ obeys the formula

$$\tan\psi(\mathbf{x},t)=-\lim_{T\to-\infty}\int_T^t\exp\left\{\int_s^t[2S_\parallel(\tau)-\delta(\tau)]\;d\tau\right\}$$
$$\times a(s)ds,$$

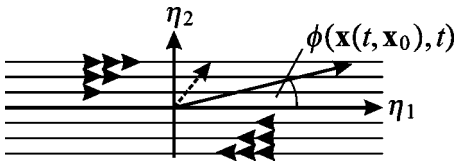

FIG. 2. For shear flows, any initial vector $\boldsymbol{\eta}_0$ aligns with the η_1 axis as $t\to\infty$.

as $t\to\infty$. Both this tracer-gradient alignment angle and the angle Eq. (11) for material alignment are exact for steady flows, as opposed to the approximate angles derived previously in the literature [8,11].

C. Ellipticity and parabolicity

If the trajectory $\mathbf{x}(t,\mathbf{x}_0)$ is periodic with period p, then

$$\mathbf{v}(\mathbf{x}(t_0,t_0))=\mathbf{v}(\mathbf{x}(t_0+p,t_0))=\boldsymbol{\Psi}(t_0+p,t_0)\mathbf{v}(\mathbf{x}(t_0,t_0)),$$

thus 1 is an eigenvalue with eigenvector $\boldsymbol{\eta}=(1,0)^T$ for the matrix $\boldsymbol{\Psi}(t_0+p,t_0)$. Consequently,

$$\int_{t_0}^{t_0+p}S_\parallel(\tau)d\tau=0 \qquad (12)$$

for any t_0, i.e., $S_\parallel(t)$ is a mean-zero periodic function. For incompressible flows, therefore, $\lambda(t,t_0)$ is a mean-zero periodic function along periodic trajectories. As a result, $\lambda(t,t_0)=0$ occurs at least twice within one period. We call this periodic recurrence of instantaneous neutral stability *elliptic* stability for the trajectory $\mathbf{x}(t,\mathbf{x}_0)$. For example, trajectories inside a vortex ring of a steady flow are elliptic.

If the trajectory $\mathbf{x}(t,\mathbf{x}_0)$ is aperiodic, a zero of $\lambda(t,t_0)$ does not necessarily lead to other zeros. In that case, a better indicator of overall neutral stability for $\mathbf{x}(t,\mathbf{x}_0)$ is the boundedness of $\eta_2(t)$ along any solution of Eq. (6). For incompressible flows, the boundedness of $\eta_2(t)$ is equivalent to

$$|\lambda(t,t_0)|\leqslant K,\qquad t\in\mathbb{R}, \qquad (13)$$

for any t_0 and for some K, as one verifies from Eq. (7). If an aperiodic trajectory satisfies Eq. (13), we say that its stability type is *parabolic*. For example, trajectories inside a jet or a shear layer of a steady flow are parabolic.

For incompressible flows, both elliptic and parabolic trajectories satisfy Eq. (13). The difference is that along parabolic trajectories with uniform shear [i.e., with $a(t)$ uniformly bounded from zero], the alignment angle $\phi(\mathbf{x},t)$ converges to zero (cf. Fig. 2), while $\phi(\mathbf{x},t)$ oscillates periodically along elliptic trajectories. Thus $|\cot\phi|\to\infty$ on parabolic trajectories, while $|\cot\phi|$ shows bounded oscillations on elliptic trajectories.

By contrast, $|\cot\phi|$ converges to a finite value along hyperbolic trajectories with $\lambda(t,t_0)>0$, and $|\cot\phi|$ tends to infinity along hyperbolic trajectories with $\lambda(t,t_0)<0$. Along the latter trajectories, we also have $\lambda(t,t_0)\to-\infty$, distinguishing them from parabolic trajectories, on which $\lambda(t,t_0)$ remains bounded by Eq. (13).

V. SLOWLY VARYING INCOMPRESSIBLE FLOWS

We now assume that the velocity field $\mathbf{v}$ is incompressible. In that case, $\delta(t)\equiv 0$ along all trajectories, and hence the coefficient matrix of Eq. (6) takes the form

$$\mathbf{A}(t)=\begin{pmatrix} S_{\|}(t) & a(t) \\ 0 & -S_{\|}(t) \end{pmatrix},$$

and Eq. (8) can be rewritten as

$$\lambda(t,t_0)=-\int_{t_0}^{t} S_{\|}(\tau)d\tau = \int_{t_0}^{t} \left.\frac{u_x(v^2-u^2)-(u_y+v_x)uv}{u^2+v^2}\right|_{\mathbf{x}=\mathbf{x}(s,\mathbf{x}_0)} ds. \tag{14}$$

Furthermore, the alignment angle $\phi(\mathbf{x},t)$ is given by the simpler expression [cf. Eq. (11)]

$$\cot\phi(\mathbf{x},t)=\lim_{T\to-\infty}\int_{T}^{t} e^{-2\lambda(t,s)}a(s)ds. \tag{15}$$

We call $\mathbf{v}$ slowly varying if the function $b(t)=\mathbf{v}^{\perp}\cdot\mathbf{v}_t/|\mathbf{v}|^2$ is small compared to the other terms in Eq. (4). By contrast, most stability studies in the Lagrangian frame assume slow variation for the full velocity gradient $\nabla\mathbf{v}(\mathbf{x}(t,\mathbf{x}_0),t)$, an assumption that already fails for typical trajectories of steady flows.

A. Slowly varying hyperbolic regions

Incompressibility implies that whenever a trajectory attracts (repels) in normal directions, it experiences stretching (contraction) in the tangential direction. As a result, both $\lambda(t,t_0)>0$ and $\lambda(t,t_0)<0$ in Eq. (9) indicate saddle-type behavior along the trajectory $\mathbf{x}(t,\mathbf{x}_0)$, at least over the time interval $[t,t_0]$. Such *finite-time hyperbolic* behavior leads to the existence of finite-time stable and unstable manifolds associated with the trajectory [9].

Under what conditions does $\lambda(t,t_0)>0$ or $\lambda(t,t_0)<0$ imply hyperbolicity for the equation of variations (4)? We answer this question below by invoking a result of Haller and Yuan [19] on the size of admissible perturbations that preserve hyperbolicity in a time-dependent linear system. We will only discuss the $\lambda(t,t_0)<0$ case, as the other case is similar.

We consider the full transformed equation of variation

$$\dot{\boldsymbol{\eta}}=\mathbf{A}(t)\,\boldsymbol{\eta}+b(t)\mathbf{B}\boldsymbol{\eta}, \tag{16}$$

and seek a condition under which Eq. (16) remains finite-time hyperbolic, provided that Eq. (6) is finite-time hyperbolic. We assume that

$$S_{\|}(t)\geqslant s_{\min}>0, \qquad |b(t)|\leqslant\epsilon,$$

for all $t\in I=[t_0,t_1]$ and for some constant $\epsilon>0$. Under the first of these assumptions, we have $\lambda(t,t_0)<0$ for all $t\in(t_0,t_1]$.

Let the matrix $\mathbf{M}(t)$ contain the normalized real eigenvectors of $\mathbf{A}(t)$. We pass to the eigenbasis of $\mathbf{A}(t)$ by setting $\boldsymbol{\eta}=\mathbf{M}(t)\mathbf{z}$, which leads to the transformed system

$$\dot{\mathbf{z}}=\boldsymbol{\Lambda}(t)\mathbf{z}+\mathbf{M}^{-1}[\dot{\boldsymbol{M}}+b(t)\mathbf{B}]\mathbf{z}, \tag{17}$$

with $\Lambda(t)=\mathrm{diag}[S_{\|}(t),-S_{\|}(t)]$. Following Haller and Yuan [19] we fix a finite time interval I and define the quantities

$$\alpha=\min_{t\in I}|\det\mathbf{M}(t)|, \quad \beta=\max_{t\in I}\|\dot{\boldsymbol{M}}(t)\|, \tag{18}$$

with $\|\dot{\boldsymbol{M}}\|=\sqrt{\Sigma_{i,j}\dot{M}_{ij}^2}$ denoting the norm of the matrix $\dot{\boldsymbol{M}}$ Note that α is a measure of the minimal angle between the two eigenvectors, while β measures the maximal rate at which the eigenvectors change.

Redefining our notation as $\dot{\boldsymbol{M}}+b(t)\mathbf{B}\to\dot{\mathbf{M}}$, we apply the results of Haller and Yuan [19] to obtain the condition

$$s_{\min}>2\sqrt{2}\,\frac{\beta+2\epsilon}{\alpha}$$

for the survival of finite-time hyperbolicity for Eq. (4) over the time interval I. Thus, we obtain the criterion

$$\left.\frac{|\mathbf{v}^{\perp}\cdot\mathbf{v}_t|}{|\mathbf{v}|^2}\right|_{\mathbf{x}=\mathbf{x}(s,\mathbf{x}_0)}<\frac{\alpha s_{\min}-2\sqrt{2}\beta}{4\sqrt{2}} \tag{19}$$

for $\lambda(t,t_0)<0$ to be a conclusive indicator of hyperbolicity for a trajectory $\mathbf{x}(t,\mathbf{x}_0)$ of the velocity field $\mathbf{v}(\mathbf{x},t)$.

For instance, if in Eq. (5) we had

$$S_{\|}(t)=2+\cos\frac{1}{2}t, \quad a(t)\equiv 1, \quad \delta(t)\equiv 0$$

along a hypothetical fluid trajectory $\mathbf{x}(t,\mathbf{x}_0)$, then we would find

$$\det\mathbf{M}(t)=\frac{2\left(2+\cos\frac{1}{2}t\right)}{\sqrt{1+4\left(2+\cos\frac{1}{2}t\right)^2}},$$

$$\|\dot{\boldsymbol{M}}(t)\|=\frac{\sqrt{\sin^2\frac{1}{2}t}}{1+4\left(2+\cos\frac{1}{2}t\right)^2}.$$

In that case, we would obtain

$$s_{\min}=1, \quad \alpha=\frac{2}{\sqrt{5}}, \quad \beta<\frac{1}{5},$$

thus the criterion (19) would be satisfied if

$$\frac{|\mathbf{v}^{\perp}(\mathbf{x}(t,\mathbf{x}_0),t)\cdot\mathbf{v}_t(\mathbf{x}(t,\mathbf{x}_0),t)|}{|\mathbf{v}(\mathbf{x}(t,\mathbf{x}_0),t)|^2}<\frac{\sqrt{5}-\sqrt{2}}{10\sqrt{2}}.$$

This last inequality then would give an upper bound on the unsteadiness of $\mathbf{v}$ for which we could rigorously conclude the hyperbolicity of the trajectory $\mathbf{x}(t,\mathbf{x}_0)$. Note, however, that Eq. (19) is only a sufficient criterion to guide one's intuition about slowness of the velocity field: if condition (19) fails, the trajectory $\mathbf{x}(t,\mathbf{x}_0)$ may still be hyperbolic.

B. Slowly varying shear regions

To conclude neutral stability from Eq. (6) for the full equation of variations (4) is more subtle. Arbitrarily small perturbations of an elliptic or parabolic trajectory may result in elliptic, parabolic, or weakly hyperbolic behavior. The growth of the alignment angle $\phi(\mathbf{x}(t,\mathbf{x}_0),t)$, however, remains an indicator of high Lagrangian shear for slowly varying velocity fields while the integral of the perturbation term in Eq. (16) is still small.

A computable finite-time expression for $\cot\phi(\mathbf{x}(t,\mathbf{x}_0),t)$ is

$$\mu(t,t_0)=\int_{t_0}^{t} e^{-2\lambda(t,s)}\left.\frac{(u^2-v^2)(u_y+v_x)-4uvu_x}{u^2+v^2}\right|_{\mathbf{x}=\mathbf{x}(s,\mathbf{x}_0)} ds, \tag{20}$$

obtained by replacing the $T\to-\infty$ limit in Eq. (15) with t_0, the earliest time at which velocity data are available.

In view of our discussion in Sec. IV C, $|\mu|$ values converging to infinity indicate uniform shear regions (i.e., overall parabolic stability) in a slowly varying velocity field. In principle, $|\mu|$ may also tend to infinity along attracting trajectories if the $\{\eta_2=0\}$ subspace remains the unstable manifold of the origin in Eq. (4). Such a coincidence is unlikely in a typical unsteady fluid flow, thus large enough values of $|\mu|$ invariably mark shear regions in applications. Large positive μ values correspond to clockwise shear, and negative μ values indicate anticlockwise shear.

VI. A NUMERICAL EXAMPLE

To test $\lambda(t,t_0)$ and $\mu(t,t_0)$ as indicators of Lagrangian hyperbolicity and shear, we consider a two-dimensional barotropic turbulence simulation used by Poje *et al.* [18] and Haller and Yuan [19]. This velocity field models the generation of mesoscale eddies in two-dimensional quasigeostrophic turbulence, and hence is an example of a geophysical flow that is considered slowly varying.

Starting at the nondimensionalized time $t_0=5$, we advect a grid of fluid particles over the planar domain $[0,2\pi]\times[0,2\pi]$ numerically. Using the definition (14), we compute and plot $\lambda(t,t_0)$ for increasing times over the initial grid positions. Local maxima of this plot will delineate the

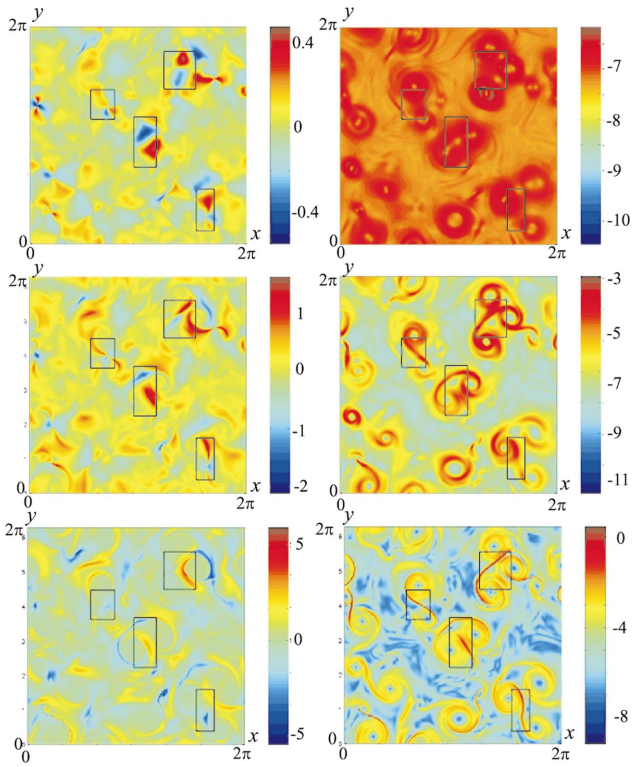

FIG. 3. (Color) Comparison of the $\lambda(t,t_0)$ field (left images) and the finite-time Lyapunov exponent distribution (right images) at times $t=5.1$, $t=5.6$, and $t=6.7$.

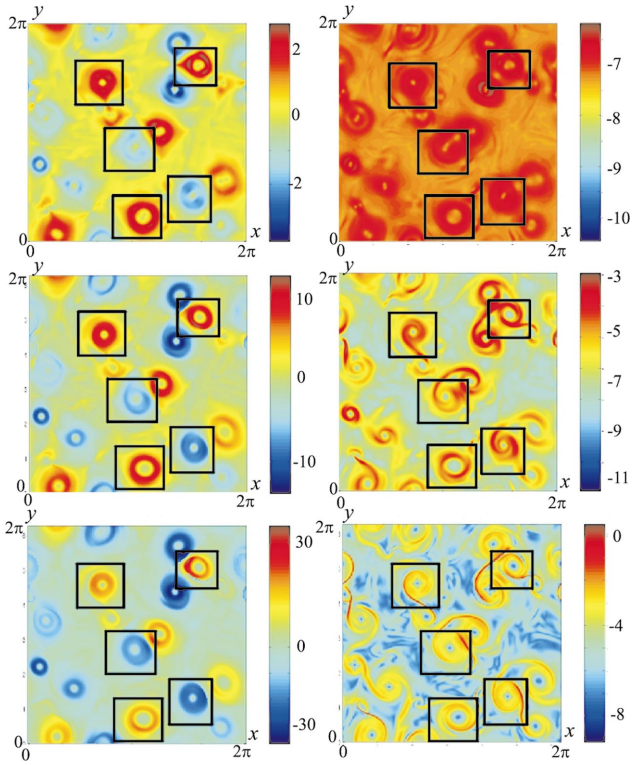

FIG. 4. (Color) Comparison of the $\mu(t,t_0)$ field (left images) and the finite-time Lyapunov exponent distribution (right images) at times $t=5.1$, $t=5.6$, and $t=6.7$.

$t=t_0$ position of material lines that repel fluid particles over the interval $[t_0,t]$. Similarly, local minima of the λ plot denote attracting material lines over the $[t_0,t]$ interval. Finally, near-zero values of $\lambda(t,t_0)$ mark material regions with neutral stability type.

We show snapshots of the above computation in Fig. 3. For reference, we also show the distribution of finite-time Lyapunov exponents calculated from the DLE algorithm described by Haller [20]. Repelling material lines and lines of high shear at $t=t_0$ both appear as maximizing curves (ridges) of the DLE plots.

Figure 3 confirms that over short time scales, the quantity $\lambda(t,t_0)$ quickly develops maxima over attracting material lines and minima over repelling material lines. By contrast, Lyapunov exponents are unable to distinguish between high-shear regions and high-stretching regions over short time scales. This is undesirable in geophysical prediction where one needs to extract repelling and attracting material lines reliably from very short datasets in order to predict the transport of material, such as chemical pollution, in real time [1]. For longer times, Lyapunov exponents become more efficient in detecting hyperbolic material lines. The inefficiency of $\lambda(t,t_0)$ over such long times is due to the growing error between solutions of the equation of variations and those of its steady limit.

Figure 4 shows snapshots of the $\mu(t,t_0)$ field defined in Eq. (20), confirming that this field indeed admits maxima over high-shear regions in slowly varying velocity fields. Again, the convergence of $\mu(t,t_0)$ is faster than that of the Lyapunov exponent field, making $\mu(t,t_0)$ the quantity of choice in geophysical prediction. Remarkably, $\mu(t,t_0)$ remains an efficient indicator of ellipticity and shear even for long times, indicating that the error between solutions of the equation of variations and those of its steady limit remains bounded.

VII. CONCLUSIONS

We have shown that the solutions of the equation of variations of a steady flow remain reliable Lagrangian stability indicators for slowly varying incompressible flows. The scalar field $\lambda(t,t_0)$ defined in Eq. (14) admits positive maxima over repelling material lines (stable manifolds) and negative minima over attracting material lines (unstable manifolds). The field $\mu(t,t_0)$ defined in Eq. (20) admits local maxima along regions of high shear, separating unmixed parcels of fluid from high-shear rings surrounding them. The $\lambda(t,t_0)$ field is most effective over short time intervals; its accuracy in Lagrangian prediction diminishes for longer times. By contrast, the $\mu(t,t_0)$ field appears to be a reliable indicator of unmixed Lagrangian vortex cores and the surrounding rings even for long times.

We have obtained the above results after a judicious choice of Lagrangian coordinates along fluid trajectories. The same choice of coordinates in three-dimensional steady flows does not lead to a solvable equation of variations, unless the flow is completely integrable. The reason is that, unlike the two-dimensional case, one solution of a three-dimensional linear system does not lead to a full general solution. Nevertheless, for three-dimensional steady flows, the solution (3) enables one to reduce the equation of variations (2) to a two-dimensional linear system that is conceptually easier to study. The implications of this reduction for slowly varying three-dimensional flows will be explored elsewhere.

ACKNOWLEDGMENTS

G.H. was partially supported by the NSF Grant No. DMS-01-02940 and AFOSR Grant No. F49620-03-1-0200. The velocity field analyzed in this paper was originally generated by Andrew Poje, who used the barotropic turbulence solver of Antonello Provenzale.

[1] F. Lekien, C. Coulliette, J. Marsden, G. Haller, and J. Paduan (unpublished).
[2] A. Okubo, Deep-Sea Res. **17**, 445 (1970).
[3] J. Weiss, Physica D **48**, 273 (1991).
[4] E. Dresselhaus and M. Tabor, J. Fluid Mech. **236**, 415 (1991).
[5] C. Basdevant and T. Philipovitch, Physica D **73**, 17 (1994).
[6] M. Tabor and I. Klapper, in *Chaos Applied to Fluid Mixing*, edited by H. Aref and M.S. El Naschie (Pergamon, New York, 1995).
[7] G. Lapeyre, P. Klein, and B.L. Hua, Phys. Fluids **11**, 3729 (1999).
[8] P. Klein, B.L. Hua, and G. Lapeyre, Physica D **146**, 246 (2000).
[9] G. Haller, Chaos **10**, 99 (2000).
[10] G. Lapeyre, B.L. Hua, and B. Legras, Chaos **11**, 427 (2001).
[11] G. Lapeyre, B.L. Hua, and P. Klein, Phys. Fluids **13**, 251 (2001).
[12] G. Haller, Phys. Fluids **14**, 1851 (2002).
[13] T.Y. Koh and B. Legras, Chaos **12**, 382 (2002).
[14] G. Lapeyre, Chaos **12**, 688 (2002).
[15] J.K. Hale, *Ordinary Differential Equations* (Kreiger, New York, 1980).
[16] R. Iacono, J. Atmos. Sci. **59**, 2153 (2002).
[17] J.M. Ottino, *The Kinematics of Mixing: Stretching, Chaos, and Transport* (Cambridge University Press, Cambridge, 1989).
[18] A.C. Poje, G. Haller, and I. Mezić, Phys. Fluids **11**, 2963 (1999).
[19] G. Haller and G. Yuan, Physica D **147**, 352 (2000).
[20] G. Haller, Physica D **149**, 248 (2001).